Mon. Not. R. Astron. Soc. **000**, 000–000 (0000) Printed 19 May 2016 (MN LATEX style file v2.2)

Line-depth-ratio temperatures for the close binary ν Octantis: new evidence supporting the conjectured retrograde planet

D. J. Ramm⋆
Department of Physics and Astronomy, University of Canterbury, Christchurch 8020, New Zealand

arXiv:1605.05453v1 [astro-ph.EP] 18 May 2016

19 May 2016

ABSTRACT

We explore the possibly that either starspots or pulsations are the cause of a periodic radial-velocity signal ($P \sim 400$ days) from the K-giant binary ν Octantis ($P \sim 1050$ days, $e \sim 0.25$), alternatively conjectured to have a retrograde planet. Our study is based on temperatures derived from 22 line-depth ratios (LDRs) for ν Oct and twenty calibration stars. Empirical evidence and stability modelling provide unexpected support for the planet since other standard explanations (starspots, pulsations and additional stellar masses) each have credibility problems. However, the proposed system presents formidable challenges to planet-formation and stability theories: it has by far the smallest stellar separation of any claimed planet-harbouring binary ($a_{\rm bin} \sim 2.6$ AU) and an equally unbelievable separation ratio ($a_{\rm pl}/a_{\rm bin} \sim 0.5$), hence the necessity that the circumstellar orbit be retrograde.

The LDR analysis of 215 ν Oct spectra acquired between 2001–2007, from which the RV perturbation was first revealed, have no significant periodicity at any frequency. The LDRs recover the original 21 stellar temperatures with an average accuracy of 45 ± 25 K. The 215 ν Oct temperatures have a standard deviation of only 4.2 K. Assuming the host primary is not pulsating, the temperatures converted to magnitude differences strikingly mimic the very stable photometric *Hipparcos* observations 15 years previously, implying the long-term stability of the star and demonstrating a novel use of LDRs as a photometric gauge. Our results provide substantial new evidence that conventional starspots and pulsations are unlikely causes of the RV perturbation. The controversial system deserves continued attention, including with higher resolving-power spectra for bisector and LDR analyses.

Key words: binaries: spectroscopic – techniques: spectroscopic – stars: late-type, starspots, oscillations – planets and satellites: individual: ν Octantis b, – planetary systems

1 INTRODUCTION

The single-lined spectroscopic binary (SB1) ν Octantis (HD 205478, HIP 107089, HD 8254; $P \sim 1050$ days), having a slightly evolved early K-type primary, has been conjectured to have a so-far unique retrograde circumstellar planetary orbit associated with it based on radial velocity observations over several years (Ramm 2004; Ramm et al. 2009). Ramm et al. more or less discounted all other standard causes for the ~ 400 day periodic signal including rotation modulation of surface features, pulsations, and a prograde orbit (which stability models indicate is rapidly unstable). Significant surface dynamics were not supported by their bisector analysis and *Hipparcos* observations (ESA 1997) had already found ν Oct to be particularly photometrically stable (see Table 1). ν Oct has been found consistently to be inactive and without significant variability at all other studied spectral regions, for instance Ca II (Warner 1969), radio (Slee et al. 1989; Beasley, Stewart & Carter 1992) and X-ray (Hünsch et al. 1996). Instrument- and data-reduction-related causes for the RV behaviour were discounted by Ramm et al. as their paper included a similar SB1, β Reticuli (K2 III; Gray et al. 2006) frequently observed on the same nights whose RVs had no such anomalous behaviour. The proposal by Morais & Correia (2012) that ν Oct is actually a hierarchical triple system has merit given how frequently such systems are anticipated and observed (Tokovinen et al. 2006; Tokovinen, Hartung & Hayward 2010). However, this scenario is challenged by the lack of observational support. In particular, their model predicts an apsidal precession rate of $-0.86^\circ/\mathrm{yr}$ for the primary star's orbit. Yet, the orbital solution for the historical RVs (which date back to 1904–1924), re-derived in Ramm (2004) and provided in Ramm et al. (2009), suggests there is no such change, since these RVs yield $\omega_1 = 82 \pm 14^\circ$ and the RVs from 2001–2006 yield $\omega_1 = 75.05 \pm 0.08^\circ$ (Ramm et al. 2009). The approximate 90-year time interval between the two datasets corresponds to about 80° of predicted precession which is not at all apparent.

Besides the possibility that ν Oct may be revealing a new type

⋆ E-mail: djr1817@gmail.com

© 0000 RAS

Parameter	ν Octantis A	Reference
Spectral type	K0 III	(3)
V (mag)	3.743 ± 0.015	(1)
$M_{\rm V}$ (mag)	$+2.02 \pm 0.02$	(2)
$(B-V)$	0.992 ± 0.004	(1)
$H_{\rm p}$ (*Hipparcos* mag)	3.8981 ± 0.0004	(3)
parallax (mas)	45.25 ± 0.25	(5)
Mass ($\mathcal{M}_{\odot}$)	1.61	(6)
Radius ($\mathcal{R}_{\odot}$)	5.81 ± 0.12	(6)
$T_{\rm eff}$ (K)	$4\,860 \pm 40$	(6)
Luminosity ($\mathcal{L}_{\odot}$)	17.0 ± 0.4	(2)
$\log g$ (g cm^{-2})	3.12 ($\pm$0.10 dex)	(6)
[Fe/H](dex)	$+0.18 \pm 0.04$	(6)
$v \sin i$ (km s^{-1})	2.0	(4),(6)
Age (Gyr)	$\sim$ 2.5–3	(6)

Table 1. Stellar and orbital parameters for ν Oct. 1: Mermilliod (1991), 2: present work, 3: ESA (1997), 4: Costa et al. (2002), 5: Ramm et al. (2009), 6: Fuhrmann & Chini (2012). The changes to several stellar parameters given in Ramm et al. (2009) by Fuhrmann & Chini for the most part originate in their increased estimate for the metallicity (shifting Eggen's (1993) value from Fe/H $= -0.11$ to their $+0.18$. Their mass errors are claimed to be likely less than 10 per cent. Their 2σ errors are halved here to be consistent with the 1σ errors used elsewhere in this study.

Parameter	Binary	conjectured planet
$\mathcal{M} \sin i$	0.55 ($\mathcal{M}_{\odot}$)	2.4 ($\mathcal{M}_{\rm Jup}$)
a (a.u.)	2.6 ± 0.1	1.2 ± 0.1
K (km s^{-1})	7.032 ± 0.003	0.052 ± 0.002
P (days)	1050.1 ± 0.1	417.4 ± 3.8
e	0.2359 ± 0.0003	0.12 ± 0.04
i ($^{\circ}$)	70.8 ± 0.9	?
ω ($^{\circ}$)	75.05 ± 0.05	260 ± 21
Ω ($^{\circ}$)	87 ± 1.2	?
N (# RV observations)	222	
RMS (m s^{-1})	19	

Table 2. Orbital parameters for ν Oct from a keplerian fit. All values from Ramm et al. (2009), except the secondary's scaled mass (Fuhrmann & Chini 2012).

of yet-to-be-determined RV-creating surface process, the remaining alternate explanation that ν Oct instead harbours this particular planet is unexpected for at least three reasons: ν Oct is substantially tighter than any other planet-harbouring binary system ($a_{\rm bin} \sim 2.6$ AU; see Table 2), the planet orbit supposedly lies about midway between the two stars ($a_{\rm pl}/a_{\rm bin} \sim 0.5$), and as a consequence, from orbit stability considerations, the Jupiter-mass circumstellar (S-type) orbit must be retrograde with respect to the binary orbit (Eberle & Cuntz 2010) where it is more likely to have long-term stability. It is the prediction that the planet orbit must be retrograde with respect to the stellar orbits that makes the ν Oct planet so far unique. This geometry is fundamentally different from the growing list of transiting exoplanets which demonstrate, via the Rossiter-McLaughlin effect, that their orbits can also be retrograde, since the R-M effect can only determine anti-alignment of a planet orbit's axis with respect to the host star's rotation axis (the first such exoplanet being HAT-P-7b: Narita et al. 2009; Winn et al. 2009). Other planets may also have retrograde orbits but their true nature is so far hidden by the circumstances of their discoveries, such as the absence of an observable R-M effect, or the absence of the demands of stability modelling as applies to ν Oct. Rather than 'simple' planet migration to explain all orbit evolution scenarios, both types of retrograde geometry imply substantial dynamical interactions can have a leading role.

The controversial geometry of ν Oct has been investigated with increasing depth beginning with Eberle & Cuntz (2010) and subsequently by Quarles, Cuntz & Musielak (2012) and Goździewski et al. (2013). Goździewski et al. explored the system in considerable detail and found that stable solutions consistent with the Ramm et al. results existed but were confined to tiny regions of the phase space. Not only is this geometry unprecedented but the formation of such a system is generally considered incompatible with theoretical expectations (e.g. Paardekooper, Thébault & Mellema 2008; Kley 2010; Thébault 2011; Rafikov & Silsbee 2015). However, the work of, for example Trilling et al. (2007), suggests otherwise. They studied infra-red excesses of close main-sequence A3-F8 binaries – encompassing the likely spectral range of ν Oct's progenitor – and found a large fraction (> 60 per cent) with small separations ($a_{\rm bin} < 3$ AU, as has ν Oct) had infrared excesses: about 50 per cent consistent with circumbinary debris discs and about 30 per cent consistent with circumstellar discs. Occasionally, the deduced debris disks were located in apparently unstable orbits. These results they claim suggests planet formation in such close binaries may not be so unlikely after all. Thus ν Oct may well be the first-discovered circumstellar consequence of such a precursor system.

At the time of writing, approximately 1500 exoplanets have been confirmed.[1] Before the upsurge of discoveries from transit-detection programs such as HATNet (e.g. Bakos et al. 2007), SuperWASP (e.g. Collier Cameron et al. 2007), and the *Kepler* mission (see e.g. Batalha et al. 2011; Rowe et al. 2014), most were discovered by the radial-velocity technique. Now the RV-detection fraction is closer to about 30 per cent of the total. Of the 120 or so evolved planet-hosting stars, two-thirds are giants and one-third subgiants, the first confirmed such examples being ι Draconis (K2 III: Frink et al. 2002), HD 47536 (K1 III: Setiawan et al. 2003), and the previously enigmatic γ Cephei A (K1 IV: Hatzes et al. 2003). Jofré et al. (2015) and Reffert et al. (2015) describe two recent analyses of large samples of evolved stars with and without planets. Approximately 10–15 per cent of claims, including ν Oct b, are unconfirmed, retracted or controversial.

The number of planets found in multiple stellar systems also continues to grow but discoveries there are less frequent, and Doppler-spectroscopic planet searches are understandably biased against binaries as tightly bound as ν Oct. A recent review of planets in such systems by Roell et al. (2012) deduced the fraction of sytems with exoplanets was then about 12% (of 477 host systems, 47 were binaries and 10 triple). Varied efforts to discover unknown stellar companions have routinely identified new components (early examples being Patience et al. 2002, Mugrauer et al. 2004, and Raghavan et al. 2006), so this fraction cannot be considered likely to be definitive. The majority of planets found in binary systems are circumstellar but a few have been identified in circumbinary (P-type) geometries e.g. HW Vir (Lee et al. 2009). More recent studies, such as SPOTS (Search for Planets Orbiting Two Stars), are specifically targeting close binary systems (Thalmann et al. 2014). SPOTS is using direct imaging to search for

[1] See e.g. The Extrasolar Planets Encyclopeadia at http://exoplanet.eu/ and Exoplanet Orbit Database at http://exoplanets.org

planets in circumbinary orbits in small-separation systems comparable to that of ν Oct ($a_{\rm bin} \lesssim 5-10$ AU).

All of the so-far-discovered circumstellar planets in multiple systems have binary separations exceeding that of ν Oct by an order of magnitude or so, and generally a lot more. The systems that are tightest ($a_{\rm bin} \sim 20$ AU) include γ Cephei A (Cambell, Walker & Yang 1988; Hatzes et al. 2003), GJ 86 A (Queloz et al. 2000), HD 41004 A (Zucker et al. 2004), and HD 196885 A (Correia et al. 2008; Thébault 2011). Interestingly, γ Cep A (which has stellar properties very similar to ν Oct- see Fuhrmann 2004), was briefly considered one of the strongest candidates for hosting the first RV-detected exoplanet until later work regrettably questioned that possibility (Walker et al. 1992), and GJ 86 Ab was one of the other earliest planet discoveries. Most recently α Cen B ($a_{\rm bin} \sim 17.5$ AU) has been claimed to host a very close planet (Dumusque et al. 2012; $P_{\rm pl} \sim 3.2$ days) but its existence has been challenged (Hatzes 2013). Other planets claimed in tight binaries, such as that for HD 188753 ($a_{\rm bin} \sim 13$ AU) were later shown to be non-existent (Eggenberger et al. 2007). None of these systems have separation ratios anywhere near as large as that claimed for ν Oct, with γ Cep, HD 196885 and HD 41004 all having $a_{\rm pl}/a_{\rm bin} \sim 0.1$.

Thus, ν Oct is the seat of one of the many unconfirmed and, in view of its geometry, perhaps most extraordinary of the controversial planets. Hence, it is appropriate that all available investigations be pursued to eliminate or support alternative explanations. Whilst Ramm et al. (2009) provided sound reasons to discredit spots and pulsation as the likely cause of the supposed planet signal, besides their bisector analysis which was inconsistent with either stellar cause, much of that reasoning was qualitative. Our effort here is to provide further quantitative evidence for the lack of support for these surface-dynamical causes.

Stellar activity in the form of spots or pulsation are expected to reveal themselves in many ways, including radial velocity, photometric, spectral-line and surface-temperature variations. The photometric stability of ν Oct has already been mentioned (ESA 1997) and recorded in Table 1. High-resolution spectra obtained for radial velocity purposes are ideal for studies of spectral-line profiles, symmetries and depths, when, as is the case for ν Oct, the spectra are uncomplicated (it is strictly SB1) and sharp-lined (due to its late spectral type and low rotation; $v \sin i = 2$ km s^{-1}: Costa et al. 2002; Fuhrmann & Chini 2012).

The most common way spectral-line variations are studied for assessing the reality of exoplanets is of the bisectors of the lines themselves (e.g. Gray 1982, 1983; Gray & Hatzes 1997) or of the cross-correlation function (e.g. Queloz et al. 2001). But measurements derived from bisection, as valuable as it is, is essentially limited to assessing the profile for asymmetry against which velocities can be compared e.g. convective velocities Gray (1982) or suspected planet signals e.g. Queloz et al. (2001). The bisector spans can also be related in a fairly general way to spectral types (Gray 1982; Gray 1992) but there is no apparent opportunity to convert these bisector spans quantitatively to a fundamental property such as effective temperature.

A star's effective temperature, $T_{\rm eff}$, is a critical parameter as it has fundamental and far-reaching consequences for many other stellar characteristics. As a consequence, many methods have been devised to measure it. In their comparison of two methods, one based on iron excitation and ionization balance and the other the infrared flux method, Tsantaki et al. (2013) list several others that include interferometry (using the relationship between diameter and luminosity), photometrically derived colour indices (which have different dependencies on temperature), and line properties such as the Hα wings, spectral synthesis strategies and, the method we will employ, line-depth ratios (LDRs). Gray (1992) also discusses various methods, including LDRs. Whilst LDRs perhaps require more reduction effort than some of these methods, they have many advantageous qualities. For instance, line depths are measured downward from the continuum so they should not suffer from zero-point errors, they should be applicable to composite spectra, and, unlike photometric methods, are independent of interstellar extinction and, within sensible limits, sky quality (Gray & Brown 2001).

Over the past couple of decades or so, many papers have been published describing the extraordinary sensitivity of ratios of the depths of suitably chosen pairs of spectral lines for a star's effective temperature. LDRs may only provide accuracy in the tens of degrees, but their sensitivity allows precision an order-of-magnitude smaller as each of the following references (and many others) will testify. Thus they provide an ideal strategy for assessing variability of $T_{\rm eff}$, and as a result of the corresponding implications for monitoring surface dynamics, a worthy tool partnered with bisectors for evaluating claimed discoveries of substellar companions.

LDRs have been used to study inactive main-sequence (e.g. Gray & Johanson 1991; Gray 1994; Kovtyukh et al. 2003), giant (e.g. Gray & Brown 2001; Kovtyukh et al. 2006), and supergiant stars (Kovtyukh 2007; Pugh & Gray 2013) as well as active stars (Gray & Baliunas 1995; Padgett 1996; Catalano et al. 2002) including the Sun's 11-year cycle (Gray & Livingston 1997). In turn, these temperatures can be used to monitor and assess starspots (e.g. active stars; Catalano et al. 2002; O'Neal 2006; Biazzo et al. 2007), pulsation cycles (e.g. of Cephieds: Kovtyukh & Gorlova 2000, and Antares A: Pugh & Gray 2013), and hence to help support claims for the non-existence or existence of exoplanets (e.g. 51 Peg; Gray 1997; Hatzes, Cochran & Bakker 1998). These latter examples demonstrate the relatively long though infrequent history LDRs have had with exoplanet research.

Our paper continues to Sect. 2 where the observational details are given, together with our reductions, choice of spectra lines and our set of LDRs. In Sect. 3 we describe the LDR construction, error management of them, and the behaviour of our LDRs with regards to ν Oct. In Sect. 4 the temperature calibration is described, and in Sect. 5 we discuss the consequences of our results that will further challenge the possibility that ν Oct's RV-perturbation might be caused by conventional spots or pulsation.

2 OBSERVATIONS AND DATA REDUCTION

The échelle spectra were obtained between 2001 and 2007 at Mt John University Observatory (MJUO), New Zealand using the 1-m McLellan telescope and HERCULES, a fibre-fed, vacuum-housed spectrograph ($P \approx 0.01$ atm; Hearnshaw et al. 2002). The spectrograph is located in a thermally isolated and insulated room. Both optical fibres used for the spectra described here have core diameters of 100 μm, one with a 50 μm microslit on its exit face, which provided resolving powers respectively of $R \sim$ 41,000 and 70,000. The detector was a 1k $\times$ 1k-pixel CCD with 24-μm pixels, which, to achieve complete spectral coverage, required four separate CCD positions. Fortunately, the position chosen to address the compromises for maximizing radial-velocity (RV) precision (the original purpose for the observations - the trade-off between spectral-line density, continuum flux and the CCD's efficiency), also recorded a useful fraction of the spectral lines often used for line-depth ratio analyses, allowing this subsequent research to be undertaken.

This CCD position recorded wavelengths $\lambda\lambda \sim 4500$–7200 Å and approximately 44 orders, $n = 81 - 124$.

The spectra were reduced using the Hercules Reduction Software Package (HRSP v.2.4; Skuljan 2004) which incorporates standard procedures, including background subtraction and cosmic ray filtering, normalization using quartz-lamp flat-field spectra following careful continuum-level definition, and wavelength calibration using a Th-Ar lamp. The flux weighted mid-time of the stellar exposures were determined using an exposure meter. The corresponding dispersion solution for each observation was determined using Th-Ar spectra obtained immediately before and after the stellar spectrum. The complete reduction created one-dimensional spectra having a wavelength range in the red (where our line-ratio lines are located) of about 50Å.

2.1 Stellar spectra

2.1.1 ν Octantis

Many of our ν Oct spectra were previously introduced in Ramm (2004), when the conjectured ν Oct planet was first mentioned, with an extended set provided in Ramm et al. (2009) when the first detailed study was reported. Since then, it has been decided that 18 of the 2009 paper's spectra are of dubious quality for precise RVs and, making no significant difference to the results to be now described, are here rejected. The reasons for these rejections were based on careful inspection of the author's observing logbook which identified several nights with suspiciously undesirable observing conditions including very poor atmospheric seeing (worse than about $7''$), Th-Ar lamp malfunctioning and failing that night, poorly timed Th-Ar calibration spectra, and/or significant observatory-control malfunctions (such as poor dome tracking). Also, significantly, the RVs of some other target stars on some of these nights also had atypical, non-random behaviour. It has also been realised that an additional 21 spectra had been acquired in 2007 but overlooked for the 2009 paper and here included.[2] Hence, a total of 225 ν Oct spectra are analysed and discussed in this paper (215 with $R \sim 70{,}000$, ten with $R \sim 41{,}000$ - the latter purely for the brief purpose of comparison of the LDRs with resolving power).

2.1.2 LDR-to-temperature calibration stars

The utility of LDRs is their ability to provide a temperature scale of extraordinary precision. Ideally, to calibrate the temperature scale as large a set as possible of spectra acquired with the same instrumentation and identically reduced is required. Given the significant influence of stellar evolution on LDRs (as the cited papers in the Introduction indicate), the calibration stars must have a similar evolutionary status ranging over an adequate temperature range with the target star's $T_{\rm eff}$ somewhere midway within that range so that reliable interpolation of temperature, rather than less reliable extrapolation, is possible. We can estimate the expected temperature variation for ν Oct based on its *Hipparcos* photometry and effective temperature $T_{\rm eff}$ given in Table 1. Assuming the primary star is not pulsating, the Stefan-Boltzmann law predicts a corresponding temperature variation of about $\Delta T = 10$ K. Thus, a set of calibration stars that have temperatures ranging over 4860 ± 500 K or so will be adequate (i.e. exceeding ΔT by 2 orders of magnitude).

Once again fortuitously, an adequate set of such spectra were discovered from past observations with HERCULES and the $1{\rm k} \times 1{\rm k}$ detector. These had also been observed during 2001–2007 with the $1{\rm k} \times 1{\rm k}$-CCD and all at $R \sim 70{,}000$, and had been acquired for the various purposes of RV templates for SB2-spectra and RV-zero-point and RV standard-star analyses (Ramm 2004). Hence, whilst sometimes a given star had only one spectrum available, it was usually of moderate–high signal-to-noise (S/N). Some properties of the 20 stars identified for this calibration task, together with ν Oct, are provided in Table 3. The V magnitudes and $(B-V)$ colour indices are from Mermilliod (1991). The parallaxes used to derive the absolute magnitudes, $M_{\rm V}$, are from van Leeuwen (2007) except for β Ret and ν Oct whose parallaxes were determined with higher precision in Ramm et al. (2009) – that for ν Oct is nearly $8\times$ more precise. The photometric variability, $\sigma_{\rm HIP}$, is taken from *Hipparcos* observations (ESA 1997). This was reviewed as a guide to identifying potentially unsuitable stars where only a small number of spectra were available but which may have had undesirable variability that was not adequately sampled with our observations. Several stars are, like ν Oct, SB1s. These include the star with the largest $\sigma_{\rm HIP} = 0.0029$, HD 219834, for which 18 spectra were chosen that had been acquired over 646 days.[3] ESA (1997) is also the source of the spectral types (G3–K2) and luminosity classes. The luminosity class of ν Oct is consistently given as III in Houk & Cowley (1975), ESA (1997), and Gray et al. (2006) though our absolute magnitude and temperature suggest it is less evolved and nearer III/IV.

The colour index $(B-V)$ was used to estimate the effective temperatures. Several relations of this type were compared in Strassmeier & Schordan (2000) in their study of LDRs of Morgan-Keenan class III giants. Of those compared the relation chosen here (from Gray 1992) was found to be of comparable accuracy to the others for our (B-V) range $\sim 0.7 - 1.2$:

$$\begin{aligned}\log T_{(B-V)_0} \;=\; & 3.988 - 0.881(B-V)_0 + 2.142(B-V)_0^2 \\ & -3.614(B-V)_0^3 + 3.2637(B-V)_0^4 \\ & -1.4727(B-V)_0^5 + 0.2600(B-V)_0^6 \,. \quad (1)\end{aligned}$$

The conversion of the $(B-V)$ values from Mermilliod (1991) to the intrinsic values $(B-V)_0$ given in Table 3 was determined using an extinction correction that does not make allowance for galactic latitude. The reasons for this decision include: 1. the stars are mostly relatively close (mean distance $\sim 70 \pm 50$ pc), 2. only two stars have a galactic latitude $< 5^\circ$ (HD 49293 and HD 109492), and only the former is beyond 100 pc, and 3. the simple isotropic formula we used predicted HD 49293's temperature to be consistent with published values (e.g. Ammons et al. 2006.) The for-

[2] The additional spectra, archived inappropriately, had been acquired over 4 consecutive nights (Feb-Mar 2007) during an unexpected exchange of CCDs when a new $4{\rm k} \times 4{\rm k}$ CCD was briefly de-commissioned and the $1{\rm k} \times 1{\rm k}$ detector returned to service. A significant revision of the $1{\rm k} \times 1{\rm k}$ spectra's RVs, acknowledging these rejections and additions, combined with a more recent large RV dataset using an iodine cell (whose lines unfortunately contaminate our LDR wavelengths) and their ongoing analysis will be the subject of a companion paper in preparation.

[3] HD 219834 has an orbital period $P = 6.3$ yrs. Its LDR behaviour at all levels of our analysis is consistent with the other calibration stars chosen, hence justifying its inclusion. The other SB1s were HD 23817 ($P = 5.3$ yrs), HD 28307 ($P = 16.4$ yrs), HD 49393 ($P = 4.8$ yrs), and HD 194215 (1 yr) (Pourbaix et al. 2004). Based on the disparity of published RVs and the author's two high-precision RVs, HD 18907 is also suspected of being an SB1 (Ramm 2004).

HD	Name	V (mag)	$M_{\rm V}$ (mag)	$\Delta M_{(\rm V-ZAMS)}$ (mag)	$(B-V)_0$ (mag)	$T_{(B-V)_0}$ (K)	Spec.	$\sigma_{\rm HIP}$ (Hmag)	#	S/N
4128	β Cet	2.04	-0.32	-7.14 ± 0.05	1.030 ± 0.009	4791 ± 19	K0 III	0.0008	6	203 ± 34
18907	ϵ For	5.88	3.34	-2.29 ± 0.05	0.798 ± 0.008	5328 ± 20	G8/K0 V(?)	0.0006	1	197
23817	β Ret	3.84	1.38	-5.90 ± 0.03	1.141 ± 0.009	4575 ± 16	K0 IV	0.0005	4	196 ± 17
25723	–	5.62	0.26	-6.84 ± 0.22	1.098 ± 0.030	4657 ± 58	K1 III	0.0008	1	199
28307	θ_1 Tau	3.84	0.46	-6.11 ± 0.09	0.963 ± 0.012	4931 ± 26	G7 III	0.0006	33	200 ± 42
35369	29 Ori	4.13	0.71	-5.99 ± 0.09	0.972 ± 0.012	4913 ± 25	G8 III	0.0004	1	473
39364	δ Lep	3.78	1.07	-5.58 ± 0.05	1.003 ± 0.013	4846 ± 27	G8 III/IV	0.0004	2	434 ± 42
49293	18 Mon	4.47	-0.80	-8.00 ± 0.23	1.141 ± 0.028	4574 ± 52	K0 III	0.0006	1	496
61935	α Mon	3.93	0.65	-6.13 ± 0.08	1.036 ± 0.013	4779 ± 25	K0 III	0.0004	1	500
80170	–	5.32	0.19	-7.37 ± 0.12	1.193 ± 0.026	4477 ± 49	K2 III	0.0004	48	203 ± 16
100407	ξ Hya	3.54	0.54	-5.97 ± 0.07	0.957 ± 0.015	4946 ± 32	G8 III	0.0006	1	379
109492	–	6.22	2.85	-2.56 ± 0.06	0.742 ± 0.012	5477 ± 33	G4 IV	0.0006	1	184
188376	ω Sgr	4.70	2.63	-2.74 ± 0.05	0.763 ± 0.007	5420 ± 20	G3/G5 III	0.0007	2	269 ± 92
194215	–	5.84	-0.09	-7.42 ± 0.31	1.137 ± 0.037	4581 ± 70	G8 II/III	0.0007	1	229
203638	33 Cap	5.36	1.03	-6.39 ± 0.14	1.178 ± 0.018	4505 ± 33	K0 III	0.0006	8	193 ± 5
205478	**ν Oct**	**3.74**	**2.02**	$\mathbf{-4.78 \pm 0.13}$	$\mathbf{0.997 \pm 0.007}$	$\mathbf{4858 \pm 14}$	**KO III**	**0.0004**	**215**	$\mathbf{204 \pm 28}$
219834	94 Aqr	5.20	3.57	-2.14 ± 0.24	0.794 ± 0.011	5338 ± 29	G6/G8 IV	0.0029	18	172 ± 17
220957	–	6.38	0.89	-5.19 ± 0.23	0.924 ± 0.032	5018 ± 71	G6/G8 III	0.0012	1	202
222803	–	6.08	1.88	-4.90 ± 0.12	1.000 ± 0.018	4853 ± 36	G8 IV	0.0007	1	202
222805	–	6.06	2.72	-3.59 ± 0.06	0.921 ± 0.011	5025 ± 26	G8 IV	0.0007	1	214
223807	–	5.75	-0.63	-8.10 ± 0.33	1.218 ± 0.046	4431 ± 86	K0 III	0.0005	1	226

Table 3. Some parameters and observation statistics for ν Octantis and the calibration stars used for the conversion of the line-depth ratios to temperatures. $T_{(B-V)_0}$ was derived using Eq. (1), # is the number of spectra used and S/N is their mean signal-to-noise. Some of our results cast suspicion on the correct spectral class of HD 18907, which appears to be evolved beyond class V (see also Footnote 3 and Footnote 4).

mula is from Henry et al. (2000): $E(B-V) = 0.8/3.3 = 0.2424\ \mathrm{mag\,kpc^{-1}}$, where $E(B-V)$ is $A_{\rm V} = 0.8\ \mathrm{mag\,kpc^{-1}}$, the interstellar V absorption, divided by the ratio of total to selective extinction.

An estimate of the stage of evolution (corresponding to a gravity index) was calculated by taking the difference between the absolute magnitude and the star's zero-age main-sequence (ZAMS) magnitude at that temperature (see e.g. Catalano et al. 2002). A cubic polynomial fit was made to the ZAMS values given in Allen (1991) and this locus was compared to the $M_{\rm V}$ vs. $T_{(B-V)_0}$ values of nearly 2000 *Hipparcos* stars within 80 pc, again using Eq. (1). The locus follows the *Hipparcos* distribution so closely that at most the only difference an alternative ZAMS locus could imply would be a minor zero-point offset which cannot effect our results significantly. The ZAMS magnitude is therefore considered to have zero error for the subsequent error estimates that will be based on standard error-propagation principles. The H-R diagram relating $M_{\rm V}$ to $T_{(B-V)_0}$ of the LDR-calibration stars and ν Oct is given in Fig. 1. The position of ν Oct is seen to be about midway between those of the calibration stars as is preferred. Another check of the suitability of the LDR-calibration stars is that all are at least two magnitudes evolved from the ZAMS. These values for $\Delta M_{(\rm V-ZAMS)}$ are given in Table 3, together with the number of spectra used and their mean signal-to-noise S/N in the vicinity of the LDR lines. For the 20 calibration stars, the average S/N is 270 ± 115. It would appear from these preliminary results that the star HD 18907 is unlikely to be properly classed as a dwarf since its high galactic latitude ($g = -61^\circ$) and proximity ($d = 32$ pc) makes interstellar reddening an unlikely complication to its H-R diagram location.[4]

[4] HD 18907 also appears better placed as a subgiant since, as will be soon become apparent, its LDR behaviour is also consistent with it being somewhat evolved.

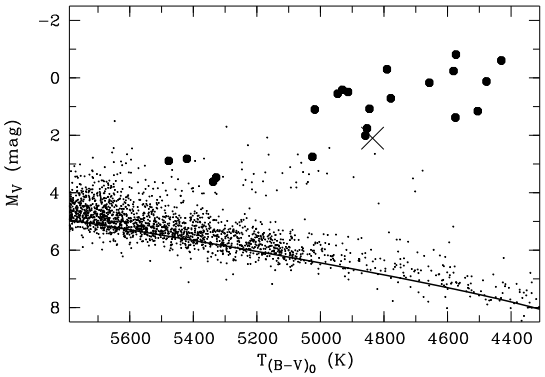

Figure 1. The absolute magnitudes and $T_{(B-V)_0}$-calibrated temperatures of 20 stars '•' and ν Octantis identified with the '×'. Approximately 2000 *Hipparcos* stars within 80 pc are included to demonstrate the adequacy of our ZAMS locus (solid line).

2.2 Spectral lines for depth ratios

Our spectra include two relatively distinct regions that include lines often used for LDR analyses. One region has the approximate range 6410–6460Å (see e.g. Strassmeier & Schordan 2000) and the other 6200–6275Å (e.g. Gray & Johanson 1991; Gray & Brown 2001; Catalano et al. 2002; Biazzo et al. 2007). Other studies examine ratios over much wider wavelength ranges e.g. Kovtyukh (2007) studied supergiants using bluer lines ranging from 5350–6080Å. Our $1\mathrm{k} \times 1\mathrm{k}$ detector restricts our choices in the 6410–6460Å range to only four lines, all of which also have a relatively high potential, $2.5 < \chi < 5.6$ eV making these a poor choice. The second re-

λ (Å)	Element	χ (eV)	label
6232.64	Fe I	3.65	6232
6233.20	V I	0.28	6233
6242.83	V I	0.26	6243
6243.82	Si I	5.62	6244
6246.32	Fe I	3.60	6246
6247.56	Fe II	3.89	6247
6251.83	V I	0.29	6252
6252.55	Fe I	2.40	6253
6255.76	Fe I	4.45	6256
6256.89	V I	0.27	6257

Table 4. Spectral lines used for line-depth ratios. Included is the integer label used in this paper.

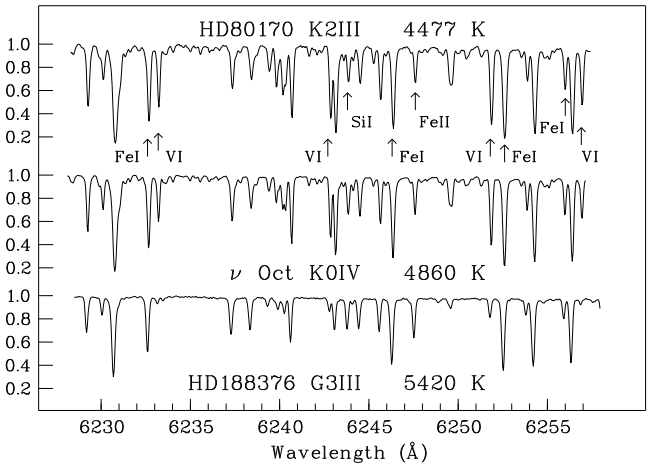

Figure 2. Three sample spectra illustrating the variations of our ratio lines with effective temperature and the resolution of them.

gion 6200–6275Å, however, includes 10 lines all recorded in one spectral order, $n = 91$, and present on all spectra.[5]

Following the recommendations of Kovtyukh et al. (2006) we selected iron-peak elements (Si, V, Fe) lines that are less gravity dependent and are expected to have less star-to-star variations in element abundances. A line's behaviour with temperature differences can be qualitatively predicted from its excitation potential, χ. The smaller the value, the greater will be the line's growth be with temperature. Four of our lines are fast-growth V I lines with low χ ($\chi_{\rm low} \sim 0.3$ eV) and the other six are slower-growth Fe I , Fe II and Si I lines with χ much higher ($\chi_{\rm high}$ in the range 2.4–5.6 eV). The nominal wavelength and excitation potential of each line, listed in Table 4, has been obtained from the VALD3 database whose original sources were Kurucz (2007, 2009, and 2013).

We constructed as many ratios as our line list permitted and ultimately selected four sets of six ratios that gave reliable correlations with $T_{(B-V)_0}$, pairing each low-χ line with one of the six higher-χ lines, all with $\chi_{\rm low}$ as the numerator. This choice ensured the T-LDR plots for our calibrations stars were always approximately linear. Inverting the ratio results in exponentially varying distributions, a more complex task for fitting regression curves. Fig. 2 illustrates the location of the lines and their behaviour with effective temperature for ν Oct and two calibration stars, the IAU RV-standard star HD 80170 (Udry, Mayor & Queloz 1999), and HD 188376. As can be seen, and is the case for all the stars studied here, the lines are very sharp indicating very low $v \sin i$ similar to ν Oct. Thus we do not expect any rotational broadening complications to our ratio measurements (see e.g. Biazzo et al. 2007). The complete list of ratios is given in Table 5, and as the paper progresses, the accompanying columns will be described.

3 LINE-DEPTH RATIO MEASUREMENTS

Each line depth, D, is derived based on the local continuum level, $S_{\rm c}$, and the line's minimum flux, $S_{\rm p}$, as determined by a parabolic fit to the three lowest bins in each line core:

$$D = 1 - \frac{S_{\rm p}}{S_{\rm c}} \, . \tag{2}$$

Strassmeier & Schordan (2000) assessed the relative merits of several techniques for this purpose (pixel minimum, parabolic fit, gaussian-fit minimum and two equivalent width strategies) and concluded in agreement with Gray (1994) that the parabolic-fit method was the most internally consistent. Using only the three lowest bins assures us that the core can be no less deep than the minimum bin value, which is not necessarily the case if more bins are used. We could restrict our analysis to lines that are close together (within an Å or so) which may minimize errors arising from the continuum estimate, but this would reduce the number of usable ratios. Furthermore, as Gray & Brown (2001) point out, amongst the advantages of measuring LDRs is that the line depths are measured downward from the continuum so they should suffer very little from zero-point errors, particularly if they are measured in a consistent manner.

Each of our spectra span about 1000 pixels. We divided this interval into 100-pixel segments and identified the pixel in each segment with the highest value. We fit a low-order polynomial to these peak values and from the coefficients determined the continuum level corresponding to each core position. Every continuum locus was assessed graphically by eye to confirm it was well-behaved.

The errors, ε, on the depth and ratio, r, are calculated as follows:

$$\varepsilon_{\rm D} = \frac{S_{\rm p}}{S_{\rm c}} \sqrt{\frac{1}{S_{\rm p}} + \frac{1}{S_{\rm c}}} \tag{3}$$

$$\frac{\varepsilon_{\rm r}}{r} = \sqrt{\left(\frac{\varepsilon_{\rm D_1}}{D_1}\right)^2 + \left(\frac{\varepsilon_{\rm D_2}}{D_2}\right)^2} \tag{4}$$

where $S_{\rm p}$ and $S_{\rm c}$ are in ADU (Analogue-to-Digital Unit).

Where more than one spectrum was available for a star, the weighted mean ratio $< r >$ for the N spectra was calculated:

[5] Doppler-shifting of the lines for our SB1s could potentially move any line close to the order edge off our detector. Attempts to use an additional two lines at $\sim$ 6266 Å were thwarted as they were not recorded after the detector exchange described in Footnote 2 and so were discarded since all ratios were wanted for all observations.

Ratio	$r_{\rm LDR} \pm \varepsilon_r$	$s_{\rm LDR}$ ($\times 0.01$ K)	$\delta T_{\rm LDR}$ (K)	$\nabla T_{\rm LDR}$ (K)	$\sigma_{\rm LDR}$ (K)	$s_{\rm MLDR}$ ($\times 0.01$ K)	$\nabla T_{\rm MLDR}$ (K)	$\sigma_{\rm MLDR}$ (K)
3332	0.626 ± 0.007	-11.0	8	-123	108	-9.1	-59	57
3344	1.184 ± 0.022	-5.4	12	-85	111	-4.4	-28	55
3346	0.561 ± 0.007	-11.7	8	-121	109	-9.7	-57	59
3347	1.226 ± 0.021	-4.8	10	-115	143	-3.7	-31	55
3353	0.503 ± 0.006	-13.2	8	-131	112	-10.9	-64	61
3356	1.183 ± 0.022	-6.9	15	-91	147	-4.9	-5	76
4332	0.852 ± 0.007	-11.3	8	-146	93	-9.0	-79	53
4344	1.611 ± 0.025	-5.2	13	-90	112	-4.0	-28	57
4346	0.763 ± 0.006	-12.1	8	-145	85	-9.7	-82	47
4347	1.669 ± 0.026	-4.6	12	-130	145	-3.4	-49	60
4353	0.685 ± 0.005	-13.7	7	-159	87	-11.0	-91	49
4356*	1.609 ± 0.025	-6.0	15	-68	222	-3.5	$+34$	113
5232	0.946 ± 0.008	-12.3	10	-151	95	-9.4	-79	57
5244	1.788 ± 0.026	-5.4	14	-85	120	-4.0	-21	65
5246	0.847 ± 0.006	-13.0	8	-150	80	-10.3	-86	48
5247	1.852 ± 0.027	-4.7	13	-133	154	-3.4	-51	67
5253	0.760 ± 0.005	-15.0	8	-168	82	-11.7	-97	49
5256*	1.786 ± 0.024	-5.7	14	-33	276	-3.1	$+67$	130
5732	0.571 ± 0.008	-10.1	8	-114	124	-8.4	-45	64
5744	1.080 ± 0.018	-5.1	9	-79	123	-4.1	-17	58
5746	0.512 ± 0.007	-10.8	8	-112	125	-9.0	-43	66
5747	1.119 ± 0.021	-4.6	10	-104	151	-3.5	-19	58
5753	0.459 ± 0.006	-12.1	7	-120	128	-10.1	-49	67
5756	1.079 ± 0.017	-6.5	11	-91	137	-4.9	-13	66

Table 5. The 24 line-depth ratios, their mean values r for ν Octantis, the slope s of the temperature-calibration-star linear fits, the implied sensitivity from those fits δT for $\Delta r = 0.01$, the corresponding differences, ∇T, for ν Oct of the mean regression temperatures from $T_{(B-V)_0} = 4860$ K, and the standard deviations σ of the calibration-star temperature differences from their $T_{(B-V)_0}$ values. The two ratios marked with '$\star$' were discarded from the final analysis.

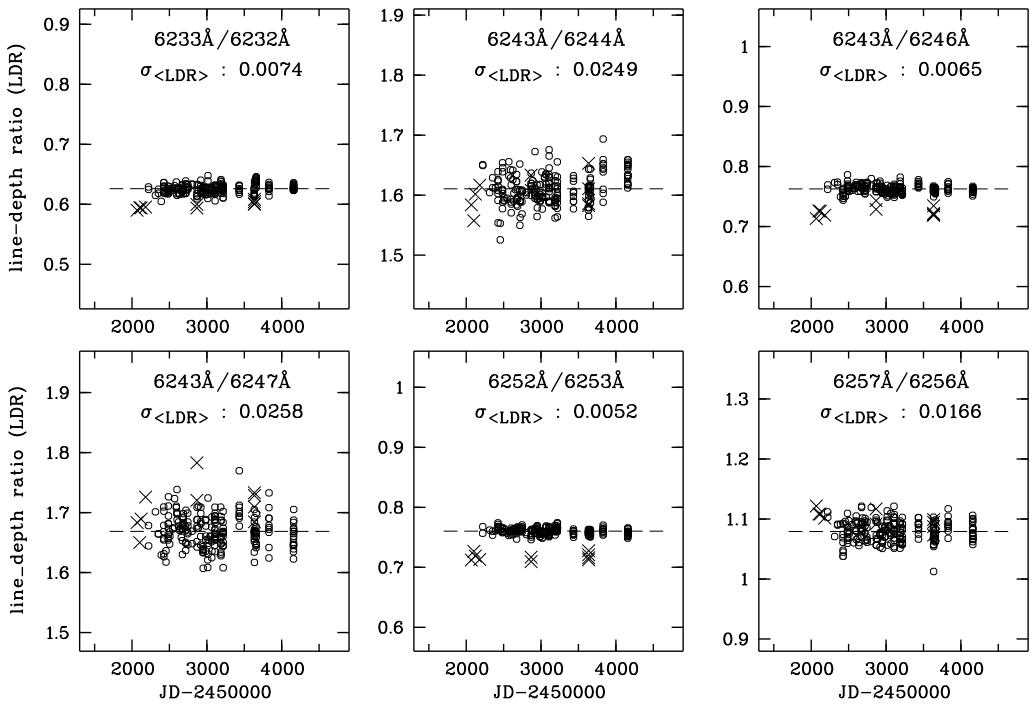

Figure 3. The time variations of a sample of six line-depth ratios typical for ν Octantis acquired between 2001–2007. The spectra are divided between ten acquired at $R \sim 41{,}000$ '$\times$', and 215 at $R \sim 70{,}000$ '$\circ$'. The standard deviation of the weighted mean for the higher resolution spectra is included. The y-axis has the same range in each plot.

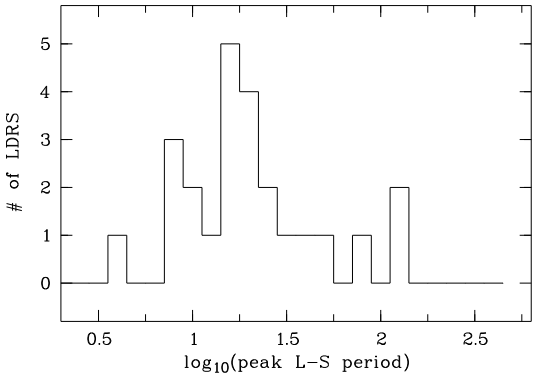

Figure 4. The distribution of Lomb-Scargle periodogram peak periods for 24 line-depth ratios. No peak has significant power above the background noise.

$$< r >= \frac{\sum_{i=1}^{N} w_i r_i}{\sum_{i=1}^{N} w_i} \tag{5}$$

where $w_i = 1/\varepsilon_{\rm i}^2$, and assuming the errors are normally distributed, the error on the mean is

$$\varepsilon_{<r>} = \sqrt{1/\sum_{i=1}^{N} w_i} \tag{6}$$

The final statistical equation used is the standard deviation of the weighted mean, which for k ratios is given by

$$\sigma_{<r>} = \sqrt{\frac{\sum_{i=1}^{k} w_i (r_i - < r >)^2}{\sum_{i=1}^{k} w_i} \frac{k}{k-1}} \, . \tag{7}$$

Six typical LDRs and their time variations for ν Oct from 2001-2007 are presented in Fig. 3. There are two significant periods we are searching for evidence of in our LDRs: 1. that of the $\sim$ 400 day RV perturbation, $P_{\rm pert}$, and 2. the rotational period of the primary star, $P_{\rm rot}$, which also remains uncertain. Our estimate for the latter is little different from the value derived by Ramm et al. (2009) since both Costa et al. (2002) and more recently Fuhrmann & Chini (2012) propose the same value for $v \sin i = 2$ km s^{-1}, but neither assign an error to it. Fuhrmann & Chini revised the radius down slightly to $\mathcal{R} = 5.8 \pm 0.12\, \mathcal{R}_{\odot}$. If we assume conservatively that the error on $v \sin i$ is ± 0.5 km s^{-1} we derive $P_{\rm rot} \simeq 140 \pm 35$ days, not dissimilar from Ramm et al. (2009). To match ν Oct's perturbation period of 400 days requires $v \sin i \sim 0.7$ km s^{-1}. If a reliable period can be found from our LDR analysis it might at least resolve this uncertainty.

As it turns out, Lomb-Scargle periodograms of the 24 LDRs revealed no evidence of any particular period consistently having a significant power exceeding the noise, and certainly not in the vicinity of $P_{\rm pert}$ ($380 < P < 420$ days) or $P_{\rm rot}$ (see Fig. 4). Twenty-one ratios have their peak power at a period < 50 days and these have an average of 18 ± 11 days. In the vicinity of $P_{\rm rot}$ ($105 < P < 175$ days) there are two ratios whose peak power falls in this range ($r4346$ and $r4353$), both having a period of about $P = 134$ days.

The results for the six ratios provided in Fig. 3 have been chosen to illustrate three with high scatter and three with low scatter. The ratio distributions, r_1 and r_2, correspond to the two resolving powers R used. The scatter is largely a result of the quotient calculation, so if the ratio was inverted, the scatter would rescale accordingly. Thus, this feature has no other particular significance. Another feature is that the difference between the means ($< r_1 > - < r_2 >$) is quite highly correlated with either ratio. For instance with $< r_2 >$, $\rho = 0.85$: the low-scatter $r < 1$ ratios have negative mean differences and the higher-scatter $r > 1$ ratios have positive mean differences. With regards our intention to obtain high-precision temperatures, one more detail has more relevance: the ratio of the standard deviations of those means, $\sigma_{\rm r_1}/\sigma_{\rm r_2}$, is approximately normally distributed, its mean being 1.0 ± 0.3. Thus, there is apparently no significant advantage for the task of getting precise temperatures for ν Oct with regards these LDRs and these two resolving powers. However, so as to avoid apparently unnecessary complications for only ten additional observations, as well as zero-point offsets that are nevertheless usually present, the lower resolving power spectra are no longer included in what follows.

Support for our strategies used to derive the depths, ratios and their errors comes from a comparison of these values for our final 215 ν Oct spectra: the standard deviation of each ratio's mean and the corresponding average error are about equal: ($\sigma_{<r>}/ < \varepsilon_{\rm r} > \sim 0.9$).

4 CONVERTING DEPTH RATIOS TO TEMPERATURES

We begin by noting that the behaviour of each line with regards to temperature is related to varying degrees to the same stellar properties that determine a star's position on an H-R diagram. These properties include its absolute magnitude, effective temperature, metallicity, age, mass, surface gravity and so on. When a simple approximate dependence (typically represented by some low-order polynomial) exists between the LDRs and, say, the temperature, the influence of other attributes create scatter about that polynomial fit. Since the exact interaction of each of these properties with each other and the LDR still has some uncertainty associated with it, we cannot hope to make an accurate allowance for any of them. Consequently, more easily and accurately determined parameters are used such as the temperature guides $(B-V)$ and $(R-I)$ indices (e.g. Flower 1996; McWilliam 1990; Gray 1992; Ramírez & Meléndez 2005), whilst for a guide to evolution, they include surface gravities, and the parameter we have already discussed - and will use - the difference between the absolute magnitude and the ZAMS magnitude, $\Delta M_{\rm (V-ZAMS)}$.

The strategy we use for the most part follows that described in Catalano et al. (2002) who studied dramatic spottedness of three recognized RS CVn-type active binaries. We will derive LDR-calibrated temperatures for all our stars, and, as a test of our accuracy, also attempt to recover the original values.[6] O'Neal (2006) has subsequently drawn attention to several concerns with regards this method when the stars have higher rotation, significant spottedness, cooler temperatures ($\lesssim 4000$ K – due to the contribution of TiO molecular bands in the LDR wavelength range employed by Catalano et al.) and inadquate spectral resolving power. We believe we will not be adversely affected by these important details as

[6] It seems inappropriate to claim we are actually checking the final 'accuracy' of our temperatures, since, even a casual review of the literature will often reveal wide variations of estimates for $T_{\rm eff}$ for each star, even for the same method of deriving it.

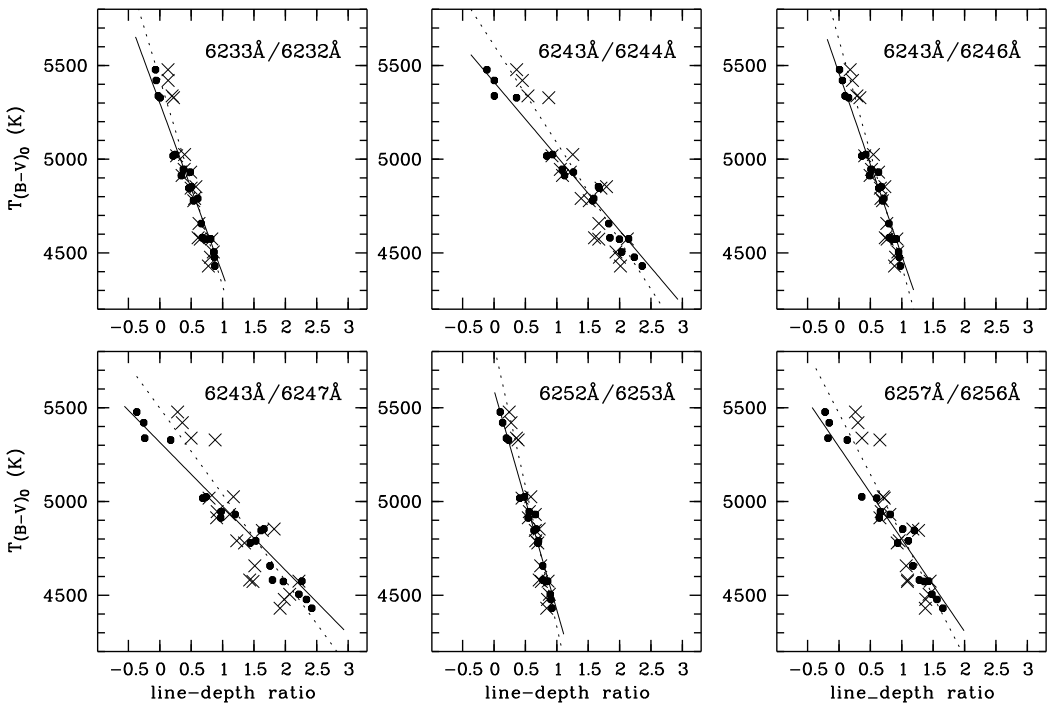

Figure 5. The variation of six typical line-depth ratios with the $T_{(B-V)_0}$ -temperatures for 20 calibration stars. The LDRs are identified with '×' and a dotted line, whilst the '•' symbols and solid line identify the modified LDRs (MLDRs) subsequently used for deriving the final temperatures for ν Octantis.

all our stars are expected to be inactive, non-spotted, slow rotators, and have $T_{(B-V)_0} > 4400$ K. Our careful inspection of our lines' behaviour with changing temperature give us confidence we have selected lines for which our methods are applicable.

For each ratio, we now plot the mean LDR for all 20 calibration stars with respect to their temperatures $T_{(B-V)_0}$ (see Fig. 5 for six typical examples, the same ratios shown in Fig. 3 for ν Oct). Two fits were derived for each ratio's data, one linear (since most ratios had this type of distribution) and the second parabolic (since a small fraction of our distributions were better fit with this function). After the analysis was carried through to its completion, it was evident that parabolic fits to the LDR-$T_{(B-V)_0}$ distributions actually gave less accurate temperature predictions for our calibration stars for all ratios. In fact this is not too surprising as LDR papers describing much wider ranges of $(B-V)$ (and hence temperature) (e.g. Strassmeier & Schordan 2000; Gray & Brown 2001), show essentially linear distributions in the range of our LDR and $T_{(B-V)_0}$ values. Therefore, the analysis that follows always uses linear fits with consideration taken for errors in both coordinates (Press et al. 2002).

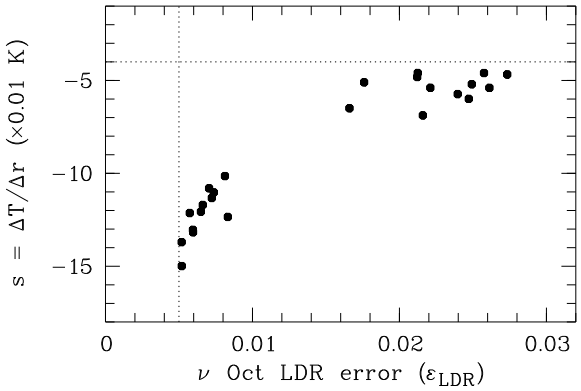

Figure 6. The relationship between the LDR calibration-star regression-line slope, s, and ν Oct's mean ratio error, ε. An LDR error bound of about 0.005 and a slope-temperature bound of about -4 K appears to be present.

4.1 Temperature predictions from LDRs

each calibration star, the regression-line temperature $T_{\rm LDR}$ corresponding to each ratio was derived, and the mean temperature from all ratios ascertained. We can judge the accuracy of the temperature predictions from this first linear fit by comparing the means, $< T_{\rm LDR} >$, of our 20 calibration stars to their $T_{(B-V)_0}$:

$$\nabla T = < T_{\rm LDR} > - T_{(B-V)_0} \ . \qquad (8)$$

The mean absolute value is 102 ± 56 K (see Table 6). This illustrates the relative weakness of raw LDRs for temperature accuracy. Our next steps, though, improve our accuracy by slightly more than a factor of two.

We can also judge the temperature sensitivity (and ultimate precision potential) of each ratio for a small shift $\Delta r = 0.01$, by calculating the slope of each LDR-$T_{(B-V)_0}$ regression line, $s_{\rm LDR} = \Delta T / \Delta r$ and multiplying its absolute value by the error on each mean ratio for the 215 ν Oct spectra, $\varepsilon_{\rm r}$ ($s_{\rm LDR}$ and $\varepsilon_{\rm r}$ are given in Table 5). This detail differs from Catalano et al. (2002)

HD	$T_{(B-V)_0}$	$\nabla T_{\rm LDR}$	$\nabla T_{\rm MLDR}$
4128	4791	91	−25
18907	5328	−219	−77
23817	4575	−50	15
25723	4657	108	46
28307	4931	19	−45
35369	4913	125	42
39364	4846	−80	−68
49293	4574	190	49
61935	4779	69	32
80170	4477	94	52
100407	4946	96	14
109492	5477	−88	−28
188376	5420	−69	−11
194215	4581	209	100
203638	4505	31	64
219834	5338	−53	67
220957	5018	79	31
222803	4853	−138	−64
222805	5025	−65	39
223807	4431	159	62
	Mean $\mid \nabla T \mid$	102 ± 56	46 ± 23

Table 6. The differences ∇T between $T_{(B-V)_0}$ and the LDR and MLDR regression-line temperatures for the 20 calibration stars.

who describe each ratio's sensitivity in terms only of the regression-line's slope. However, as Fig. 6 illustrates (at least for our stars), there is a relatively strong relationship between this calibration-star slope, s, and the ν Oct-ratio errors:

$$\delta T = \mid \frac{\Delta T}{\Delta r} \mid \times \varepsilon_{\rm r} = s \times \varepsilon_{\rm r} \simeq \text{ constant} . \qquad (9)$$

This 'constant' averages 10 ± 3 K. We also see there is an apparently limiting mimimum error, $\varepsilon \sim 0.005$, which is presumably set by our methods (resolving power, S/N, ratio measurements) and an apparently limiting minimum slope, s, which is at about -4 K for the $r_{\rm LDR}$ distribution. That the relationship in Eq. (9) appears to exist is very desireable as it implies *we are measuring much the same temperature variations of* ν Oct *with all our ratios*, as in fact ideally we should be. This is would also seem to be an important detail for our final temperature-precision claims. The δT values are also given in Table 5 and indicate, even at this stage in our analysis, individual ratio sensitivities lie between $7 - 15$ K.

Our 215 ν Oct spectra and 24 LDRs provided 5160 temperatures. The corresponding errors were estimated using the calibration-star-LDR slope and LDR error: $\varepsilon_{\rm T} = \varepsilon_{\rm r} \times \Delta T / \Delta r$, the average error being 12 ± 3 K. Rather than tabulate the mean temperature for each ratio we provide in Table 5 their differences from our expected value ($T_{(B-V)_0} = 4858$ K). These differences, all of which indicate an underestimation of the temperature relative to $T_{(B-V)_0}$, have a mean of -115 ± 33 K, a similar level of accuracy as found for the calibration stars for our LDR treatment. Finally, for each ratio in Table 5, the regression-line temperatures for the calibration stars are compared to their $T_{(B-V)_0}$ values and the standard deviation, σ, of their differences included. Two ratios, $r4356$ and $r5256$, stand out as relatively poor examples for recovering the original temperatures, since the associated standard deviations, $\sigma_{\rm LDR}$, exceed 220 K whilst the remainder have a mean 120 ± 20 K (see Table 5).

4.2 Improving the regression-line predicted temperatures

The next step is to derive a second linear fit, with y-intercept a and slope b, this time to the residuals of the LDR-$T_{(B-V)_0}$ fit, but now in relation to $\Delta M_{\rm (V-ZAMS)}$. This step brings our second H-R diagram coordinate into play. Examples of two such distributions are given in Fig. 7. These two examples (for $r5246$ and $r5247$), which are close to the extremes for scatter, were chosen to show two other features: 1. the scatter of LDR residuals to $\Delta M_{\rm (V-ZAMS)}$ varies considerably and is independent of the wavelength separation of the lines used for the ratio, and, 2. these and all other distributions have a small and positive slope indicating there is a remaining sometimes well-defined but incompletely-corrected correlation between the LDR and our evolution index. We assume the greater scatter of the distributions for some ratios represents their greater sensitivity to effects not yet adjusted for (surface gravity, metallicity and so on). The two ratios with the highest scatter include the Fe I line 6256Å – $r4356$ and $r5256$. The next four highest scatters are for ratios including the Fe II line 6247Å. This latter result is consistent with findings commented upon by Catalano et al. (2002), whose two LDRs including this line ($r4347$ and $r4647$) had such high gravity-dependence that they could not be used for all of their calibration stars. Similarly, our ratio $r5253$ shows a very small scatter and Catalano et al. illustrated the tiny gravity effect this ratio has by the near coincidence of their main-sequence and giant star calibration curves.

This second linear fit provides the final step to our temperature calibration and is often referred to as a 'correction' to the LDR, but we prefer to label it as a 'modification'. The absolute-magnitude modified LDR, which we label MLDR, is given by the simple expression

$$r_{\rm MLDR} = r_{\rm LDR} - (a + b\,\Delta M_{\rm (V-ZAMS)}) . \qquad (10)$$

The distributions and the linear-regression fits of six of these modified LDRs are included in Fig. 5. It can be seen that each MLDR line has less scatter and also less slope than the respective LDR distributions. The improvement to the accuracy of our mean regression-predicted temperatures of our 20 calibration stars is significant (see Table 6). Now $\mid < T_{\rm MLDR} > - T_{(B-V)_0} \mid \sim 46 \pm 23$ K, which is slightly better than half the corresponding value given in § 4.1 from the LDRs, and serves as an indication of the final accuracy of the temperature scale we will apply to our ν Oct analysis.

4.3 Final temperatures for ν Octantis

The MLDR for each ν Oct observation was created using Eq. (10) and these converted via the calibration-star-regression to the 5160 temperatures for our 215 spectra. The calibration-star-regression slopes, s, and temperature differences between our ν Oct $T_{(B-V)_0}$ and $T_{\rm MLDR}$ values, ∇T, are added to Table 5. The differences ∇T are significantly reduced.

Before proceeding it is now appropriate to review all the ratios and decide if any can justify rejection. Most of the papers we cite comment upon the presence of ratios they deem suitable for rejection initially or as their analyses progess. For instance, the metallicity dependency of lines and their ratios is a function of the degree of their saturation, weak lines having almost no metallicity dependence (Gray 1994). Since we have made no adjustment for metallicity, we might expect our ratios using a more saturated line (such as at 6253Å) might yield poorer accuracy and so war-

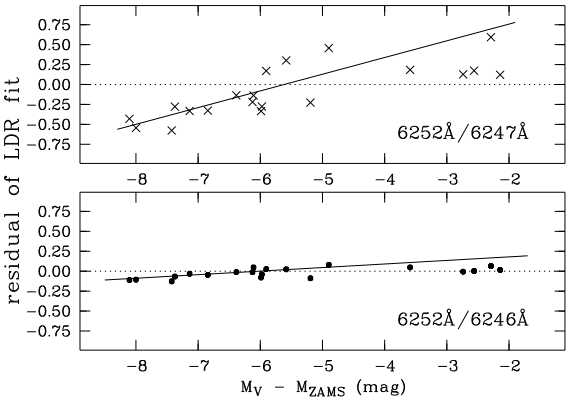

Figure 7. Two examples of the distribution of residuals of the linear fits to $T_{(B-V)_0}$-LDR in relation to our evolution index $\Delta M_{(\mathrm{V-ZAMS})}$. For each ratio a second linear fit was calculated (the sloping solid lines shown here) that created the modified ratio (MLDR) used to derive our final temperatures.

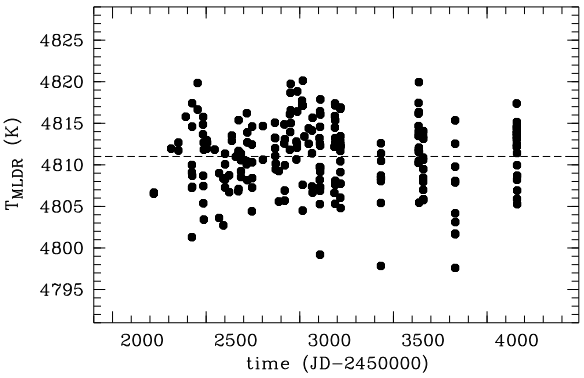

Figure 8. The final MLDR-calibrated temperatures for ν Octantis. The mean is 4811.0 ± 4.2 K.

rant rejection. This dependency is not evident from our results and helped us decide not to include a metallicity adjustment for our LDRs.[7] However, two ratios, $r4356$ and $r5256$, were identified in our LDR analysis as having the least accuracy recovering the original $T_{(B-V)_0}$-calibrated temperatures. This weakness continues with the MLDRs. The other 22 ratios have a fairly tight mean standard deviation for the calibration-star temperatures of 59 ± 7 K, whereas $\sigma_{\mathrm{MLDR}} > 110$ K, or at least 7σ, for these two less accurate ratios (see Table 5). They are therefore discarded from the final analysis.[8]

As the ∇_{MLDR} values in Table 5 demonstrate, there are zero-point offsets between the regression-line temperatures (T_{MLDR}, i.e. using the solid lines as in Fig. 5) from our remaining 22 ratios ($\sigma = 27$ K). The mean temperature for each ν Oct observation from these ratios was calculated without any arbitrary zero-point adjustment. This decision is the only sensible one given our goal to assess the likely true variability of our dataset. Adjusting for the offsets can be expected to only unfairly reduce the scatter. The mean temperature from the 22 ratios, $T_{\nu Oct} = 4810 \pm 27$ K, is consistent with the published effective temperature (Fuhrmann & Chini 2012) who found $T_{\mathrm{eff}} = 4860 \pm 40$ K. It is also consistent with the accuracy of our mean regression-predicted temperatures of our 20 calibration stars, 46 ± 23 K, as mentioned above. The MLDR-calibrated temperatures for the 215 ν Oct spectra, now taking the weighted mean of the 22 ratio temperatures for each spectrum, are illustrated in Fig. 8. Their standard deviation is only 4.2 K. Not surprisingly, given the lack of support for any significant periodicities in our original LDRs (see § 2.2), once again a Lomb-Scargle periodogram reveals no significant power above the general noise at any period.

[7] Another reason was the considerable variation of metallicity values for any star apparent from a review of values in such databases as VizieR. Indeed, ν Oct has had its [Fe/H] recently revised from -0.11 (Eggen 1993) to $+0.18$ by Fuhrmann & Chini (2012), a difference that is not at all unusual between different studies.

[8] These are the only ratios that have $\nabla_{\mathrm{MLDR}} = T_{\mathrm{MLDR}} - T_{(B-V)_0} > 0$ showing they appear to make the star too hot from this pair. Gray (1994) also comments on this related detail.

5 DISCUSSION

Our results so far provide no evidence for significant surface temperature variations that are presumably essential evidence of either spots or pulsation to be the cause of the $\sim$ 400 day RV-perturbation of ν Octantis. Another diagram provides further evidence, this time pushing our claims back to the observations of *Hipparcos* (ESA 1997). If we assume ν Oct is not pulsating i.e. $\Delta\mathcal{R} = 0$, we can derive the corresponding magnitude variations, Δm, using $M_{\mathrm{bol}_2} - M_{\mathrm{bol}_1} = -2.5 \log(L_2/L_1)$. We create ratios of all our MLDR temperatures with their weighted mean i.e. $T_{\mathrm{MLDR}}/T_{\nu Oct}$. Since the bolometric correction can be sensibly assumed to be constant for our tiny temperature variations, and the challenging decision of how to define the stellar radius disappears with the ratio, returning to the Stefan-Boltzmann law, $L_2/L_1 = (R_2/R_1)^2 (T_2/T_1)^4$, we have

$$\Delta m = -10 \, \log \left(\frac{T_{\mathrm{MLDR}}}{T_{\nu Oct}} \right) . \qquad (11)$$

These values are plotted in Fig. 9 together with the Δm values derived from the *Hipparcos* observations, $\Delta m = H_{\mathrm{obs}} - H_{\mathrm{p}}$, where H_{p} is given in Table 1, and both datasets are shifted to the same zero-point $\Delta m = 0$. The distribution of MLDR-predicted magnitudes of course duplicates the temperature distribution in Fig. 8 (though now inverted as a cooler temperature corresponds to a more positive magnitude). The striking similarity of our Δm magnitudes to the *Hipparcos* magnitudes implies the primary star of ν Oct has the same distribution of brightness variations as it did $\sim$ 15 years previously. This useful result further justifies extending our analysis from one of only LDRs to the more complex one that has converted the LDRs to temperatures. The brightness variation is very sensitive to the temperature ratio: increasing the temperature range by one degree increases the magnitude range by about one millimag, so even increasing ΔT by a mere 10 K would make a significant change to our Δm distribution. Such a close match for this high-precision behaviour seems highly unlikely to be coincidental – presumably the star is behaving the same way in 2001–2007 as it did from 1990–1993.

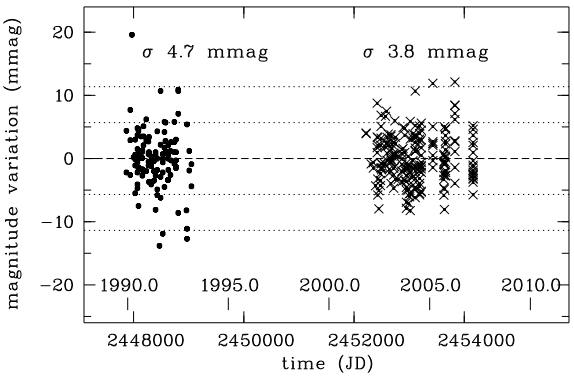

Figure 9. The implied brightness variation, Δm, of ν Oct based on our MLDR-calibrated temperature variations '$\times$' compared to the brightness variations recorded by *Hipparcos* '$\bullet$' (only the 116 best-quality flag $= 0$ observations included). The dotted lines identify the $\pm 1.5\sigma$ and $\pm 3\sigma$ limits from our MLDR predictions.

5.1 Pulsations

Variability amongst K-giants is well recognized, with many having photometric and RV periodicities of several hundred days and RV semi-amplitudes up to and sometimes in excess of 100 $\mathrm{m\,s^{-1}}$ (Walker et al. 1989; Cummings et al. 1999; Henry et al. 2000). The RV period can be comparable to the K-giant rotation period and this detail alone should sound alarm bells for the controversial ν Oct planet. Ramm et al. (2009) noted this detail, but also that the $(B-V)-M_{\rm V}$ position of ν Oct places it neatly in the space of more typically 'RV-stable' K giants ($\sigma_{\rm RV} \lesssim 20$ $\mathrm{m\,s^{-1}}$; see e.g. Henry et al. 2000, Hekker et al. 2006). Here we investigate the likelihood of pulsations based on our LDR results.

By integrating the near-sinusoidal perturbation RV curve we can estimate the change to the star's radius based on the semi-amplitude $K_{\rm RV}$ and period $P = 400$ days. A highly eccentric orbital solution argues in favour of a planetary cause (see e.g. the case for the K2 III ι Dra; Frink et al. 2002), but the small non-zero eccentricity calculated for the conjectured ν Oct planet ($e \sim 0.1$) is no obstacle. Also, Ramm et al. (2009) have assumed their RVs fit a Keplerian orbit (which in any case may be a significant oversimplification), so it is not surprising that some non-zero eccentricity has been derived. We assume $e = 0$ and therefore $\Delta\mathcal{R} = K_{\rm ps}P/2\pi = p_{\rm c}K_{\rm RV}P/2\pi$, where $p_{\rm c} = K_{\rm ps}/K_{\rm RV} = 1.39$ is a projection correction factor for estimating the pulsation velocity amplitude $K_{\rm ps}$ (Nardetto et al. 2006). For K in $\mathrm{m\,s^{-1}}$, $\Delta\mathcal{R} \sim 0.011K_{\rm RV}$ $\mathcal{R}_\odot$. So for every increment of 10 $\mathrm{m\,s^{-1}}$ with $K_{\rm RV}$, the predicted change to the star's radius is about 0.1 $\mathcal{R}_\odot$ which acting alone corresponds to a brightness change of about 40 mmag. This is far in excess of any compensating contribution our small temperature variations could provide (i.e. merely a few millimag). Indeed, the necessary temperature change to offset the brightness change with $\Delta\mathcal{R}$ is about 40 K for every 10 $\mathrm{m\,s^{-1}}$ increase in $K_{\rm RV}$. These temperature changes would have to be in-phase with the radius changes (otherwise the brightness would be more variable), which itself is inconsistent with recognized classical pulsation behaviour where temperature changes typically significantly lag velocity changes (see e.g. Kurtz 2006; Pugh & Gray 2013). Thus, there is no support for conventional pulsations as the cause of the ν Oct RV perturbation from our LDR analyses.

5.2 Starspots

For starspots to cause the RV perturbation, the primary star would have to have those spots suitably distributed on the observer-facing pole, one spot group if the rotation period $P_{\rm rot}$ matched the perturbation period $P_{\rm pert} \sim 400$ days, and two groups fortuitously separated by 180° if $P_{\rm rot} = 2P_{\rm pert}$, as Ramm et al. (2009) noted. Such 'fortuitous' spot geometries have been identified in the active longitudes of other stars (see e.g. Järvinen et al. 2005; Gray & Brown 2006). In any case, in § 2.2 we found $P_{\rm rot} \sim 140$ days, and its published radius and $v \sin i$ (see Table 1), at least imply $P_{\rm rot}$ is not likely to exceed 200 days.

But it is again not clear that our temperature variations, if now from spots, are capable of producing the RV perturbation unless we convert the temperatures to some estimate of spot geometry and subsequently RV behaviour. We define the filling factor f(%) as the ratio of the total spot area A_s to the visible hemisphere area A_v. We can derive various equations in terms of $f = 100 \times A_s/A_v$ and the unspotted photosphere temperature (assumed to be the maximum observed) $T_{\rm ph}$, the integrated observed mean temperature $T_{\rm obs}$ when cooler spots are on the visible hemisphere, and the spot temperature $T_{\rm s}$. The difference between $T_{\rm obs}$ and $T_{\rm ph}$ corresponds to the brightness variation Δm. O'Neal (2006) discusses the difficulties inherent in calculating a 'meaningful' average temperature when spots are involved. In any case, we have our empirical temperatures $T_{\rm obs}$ so calculating them is unnecessary. O'Neal also emphasises concerns for using LDRs to measure spot temperatures $\lesssim 4000$ K. Our analyses so far, and what now follows, suggests these particular concerns are not relevant here.

We estimate the filling factor in a relatively simple manner that should give sensible order-of-magnitude predictions of what we are now exploring. In the first place, the ratio of the spotted and unspotted luminosities, L_2 and L_1 respectively, is given by

$$\frac{L_2}{L_1} = \frac{(A_v - A_{\rm s})T_{\rm ph}^4 + A_s T_{\rm s}^4}{A_v T_{\rm ph}^4} = 1 - \frac{f}{100}\left[1 - \left(\frac{T_{\rm s}}{T_{\rm ph}}\right)^4\right] . \quad (12)$$

By application of the Stefan-Boltzmann law (since again we assume $\Delta\mathcal{R} = 0$) we can then derive

$$\frac{f}{100} = \frac{1 - 10^{-0.4\Delta m}}{1 - (T_s/T_{\rm ph})^4} \quad (13)$$

and

$$\frac{f}{100} = \frac{T_{\rm ph}^4 - T_{\rm obs}^4}{T_{\rm ph}^4 - T_s^4} \quad (14)$$

since L_2/L_1 also equals $(T_{\rm obs}/T_{\rm ph})^4$. Eq. (14) allows estimation of f when empirical temperatures are available such as we have from our MLDR calibrations, and would show the filling factor changing in a non-periodic manner consistent with our temperature distribution.

Eq. (13) is useful for estimating maximum f when a given brightness constraint exists, such as we have demonstrated in Fig. 9. The standard deviation of the brightness variations from *Hipparcos* (which cannot be seriously questioned) and our MLDRs (which are based on very precise temperatures and the sensible alternative $\Delta\mathcal{R} = 0$) are both $\Delta m \sim 4$ mmag which bounds about 70 per cent of our MLDR datapoints. Extending the boundary to

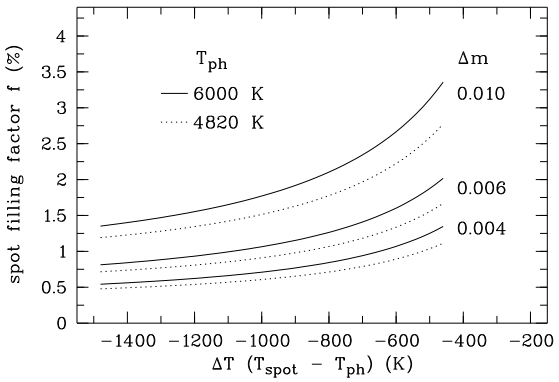

Figure 10. The predicted spot filling factors created by Eq. (13) corresponding to two unspotted photosphere temperatures $T_{\rm ph}$ and three brightness variations Δm (mag).

$1.5\Delta m \sim 6$ mmag includes 90 per cent of them. Both limits are included in Fig. 10, which illustrates the variation of f for three values of Δm, a wide range of spot temperatures, and two photosphere temperatures $T_{\rm ph}$ including the maximum MLDR-calibrated temperature we derived for ν Oct, 4820 K. These two temperature curves demonstrate the influence of $T_{\rm ph}$. Each value for Δm plotted in Fig. 9 creates its corresponding estimate for f. At these very low values for Δm, f is not very senstitive to $T_{\rm ph}$.

With regards our plan to estimate spot-induced RV predictions, we utilise the work of Hatzes (2002), who also used a photosphere temperature of 6000 K. However, the Hatzes analysis was specifically for cool spots on sun-like stars. Thus, spottedness of a different nature cannot be reliably assessed in what follows. For $-1400 < \Delta T < -800$ K, expected to be typical for many spots (see e.g. Biazzo et al. 2006; O'Neal 2006), each filling factor curve varies very little, and less so for greater $\mid \Delta T \mid$. For any photosphere temperature $4800 \leqslant T_{\rm ph} \leqslant 6000$ K and $\Delta m \leqslant 6$ mmag, we find f does not exceed about 1%. The RV-amplitude prediction from Hatzes (2002) for this low filling factor and $v \sin i = 2$ km s^{-1} is $\lesssim 15$ m s^{-1}. Also, $K_{\rm RV}$ is approximately proportional to $v \sin i$ for our model values, so an unrealistic increase to $v \sin i$ would be required to approach the order of magnitude of $K_{\rm pert}$. That this signal is not evident in our temperature distribution, and hence neither in our predicted f distribution (there is no hint of the required rotation-modulated periodicity), and since our predicted spots seem incapable of producing the observed RV perturbation, supports – now quantitatively with data from the same time interval – the claim of Ramm et al. (2009) that cool spots are unlikely to be the perturbation's cause.

6 CONCLUSIONS

This paper confirms the extraordinary temperature precision achievable from line-depth ratio analyses, in this instance for the K0 III/IV primary star in the SB1 ν Octantis. An important consequence is that the conjectured circumstellar retrograde planet of this unusually tightly bound system has further support. If it wasn't for the close stellar companion, it would be unlikely that the ν Oct planet would be in question given the range of standard tests so far applied and passed, and which now includes the sensitive but less frequently used LDR strategy.

Twenty similarly-evolved calibration stars and 24 ratios from high-resolution spectra were examined resulting in a final set of 22 ratios providing very consistent results. When compared to temperatures derived from the intrinsic colours, our MLDR-calibrated temperatures for both our calibration stars and ν Oct, recover our original $T_{(B-V)_0}$ temperatures typically to within about 45 K. Our final 215 temperatures for ν Oct, spanning several years of observations (2001–2007), predict $T = 4811$ K with a standard deviation of only 4.2 K. The published effective temperature is 4860 ± 40 K (Fuhrmann & Chini 2012).

These results provide the first quantitative evidence that the primary star in ν Octantis has no significant temperature variability during the six-year observation window. In particular, there is no evidence for any significant periodic behaviour in the LDRs anywhere near the star's expected rotation period $P_{\rm rot} \sim 140$ days nor near the RV-perturbation's period, $P_{\rm pert} \sim 400$ days, the latter suspected of being caused by a retrograde planet. When converted to brightness variations, our temperatures imply the star is unchanged since its very low-variablity observations by *Hipparcos*, ~ 15 years previously (ESA 1997). Thus we have also demonstrated a novel and revealing use of LDRs as a photometric gauge.

The ability of LDRs to examine a fundamental property such as temperature and its many ramifications, as we have initiated for the case of ν Oct, should serve as a reminder that LDRs presumably deserve more widespread use to help elucidate the true nature of other exoplanet candidates, perhaps particularly but certainly not limited to those that are also controversial, challenged or extraordinary in some way.

These results more strongly support the conclusions of Ramm et al. that conventional spots and pulsations are unlikely to be the cause of ν Oct's RV-perturbation. A prograde orbit has no stability, and the binary-secondary scenario proposed by Morais & Correia (2012) appears to be unsupported by the available orbital solutions. Therefore the only recognizable astrophysical scenario continuing to be consistent with all available data is a retrograde planet (Ramm et al. 2009; Eberle & Cuntz (2010). Thus, the reality of a planet in this unusually tight binary system's geometry ($a_{\rm bin} < 3$ AU, $a_{\rm pl}/a_{\rm bin} \sim 0.5$) has more credibility and, for the time being, becomes that much more controversial.

Our study appears to be sufficiently robust that it would seem difficult to explain the star's temperature stability if in the future surface dynamics were instead identified as the cause of ν Oct's RV behaviour. Such a result would imply that the RV behaviour is caused by a similarly unexpected cause, namely a new type of RV-creating surface process that has, in terms of our present knowledge, conflicting characteristics - namely be able to create a significant RV signal without any photometric, LDR nor bisector evidence.

Of course new surface phenomena can be imagined to properly explain new empirical evidence. Such an example of a variation of otherwise common stellar surface features (namely sunpots and starspots) are the low-contrast 'starpatches' proposed by Toner & Gray (1988). Similarly, Hatzes & Cochran (2000) investigated the possibility of 'macroturbulent' spots for the behaviour of Polaris (where the spot was distinguished by having a substantially lower macroturbulent velocity than the surrounding surface). However, predictions of such new phenomena have their own risks, since these can in turn be erroneous. For instance, in a detailed analysis of 51-Peg spectra ($R \sim 100{,}000$) which included LDRs and bisectors, Gray (1997) and Gray & Hatzes (1997) proposed that a better alternative to that planet (Mayor & Queloz 1995) seemed to be a new mode of stellar oscillation in solar-type stars. How-

ever, using $R \sim 220{,}000$ spectra, Hatzes et al. (1998) were able to help confirm the now-accepted reality of the planet. This should provide a warning for the challenges inherent in using even spectra with R as high as 100,000 for bisector and LDR analyses. Of course, a large fraction of planets have been both supposedly confirmed and others refuted with spectra of only modest resolving power. For instance, HD 166435's planet was refuted in a frequently cited paper by Queloz et al. (2001) with spectra having only $R \sim 42{,}000$. Indeed it remains unclear just what minimum resolving power is reliable for bisector and LDR studies in each instance, and, specifically, it remains to be proven if the spectra used by Ramm et al. (2009) for their bisector analysis, and again used here ($R \sim 70{,}000$) are in fact truly adequate to reveal the tell-tale evidence of a non-planetary cause. This detail perhaps remains the biggest obstacle for greater confidence that the extraordinary ν Oct planet is real.

If proposals of new surface behaviour are possible for solar-type stars, it is surely possible for evolved stars about which we have less certain knowledge. However, if our increasing list of reasons to support the reality of the ν Oct planet is confirmed, such as of the lack of suitable bisector and LDR variability with higher resolving-power spectra, should the controversial planet be later disproven by the discovery of another cause, it would presumably have serious implications for many exoplanet claims.

The challenges the ν Oct system presents for its formation are formidable and challenging for long-term stability theories as well. But unless somehow discredited in the future, the ν Oct system will be a prime motivator for studying such demanding geometries. Besides being consistent with the debris-disk proposals in similar close binaries as mentioned in our Introduction (i.e. by Trilling et al. 2007), perhaps the ν Oct planet will be a suitable candidate for such histories as 'star-hopping', whereby a planet in a binary, rather than being ejected by collisions from a passing star or strong interactions from close stellar companions or an evolving stellar host, instead is exchanged between the stars (see e.g. Kratter & Perets 2012). Such an exchange may explain the proposed retrograde orbit.

ACKNOWLEDGMENTS

The author thanks the referee, A. Hatzes, for his reading of the paper and his helpful comments. The author is grateful for the availability of 18 spectra acquired by S. Komonjinda, J. Skuljan and J. Hearnshaw. This work benefited from NASA's Astrophysics Data System, the SIMBAD database and the VizieR catalogue access tool, CDS, Strasbourg, France, and the Vienna Atomic Line Database (VALD3).

REFERENCES

Allen C. W., 1991, Astrophysical Quantities, 3rd ed., The Athlone Press, London
Ammons S. M., Robinson S. E., Strader J., Laughlin G., Fischer D., Wolf A., 2006, ApJ, 638, 1004
Bakos G. . et al., 2007, ApJ, 656, 552
Batalha N. M. et al., 2011, ApJ, 729,
Beasley A. J., Stewart R. T., Carter B. D., 1992, MNRAS, 254, 1
Biazzo K., Frasca A., Catalano S., Marilli E., Henry G. W., Tăs G., 2006, MSAIS, 9, 220
Biazzo K., Frasca A., Catalano S., Marilli, E., 2007, AN, 328, 938
Campbell B., Walker G. A. H., Yang S., 1988, ApJ, 331, 902
Catalano S., Biazzo K., Frasca A., Marilli E., 2002, A&A, 394, 1009
Collier Cameron, A., et al., 2007, MNRAS, 375, 951
Correia A. C. M. et al., 2008, A&A, 479, 271
Costa J. M., da Silva L., Nascimento J. D. Jr., de Medeiros J. R., 2002, A&A, 382, 1016
Cummings I. N., Hearnshaw J. B., Kilmartin P. M., Gilmore A. C., 1999, in Hearnshaw J. B., Scarfe C. D., eds, ASP Conf.Ser.Vol.185, Precise Stellar Radial Velocities, Astron.Soc.Pac., San Francisco, p. 204
Dumusque X., et al., 2012, Nature, 491, 207
Eberle J., Cuntz M., 2010, ApJ, 721, L168
Eggen O. J., 1993, AJ, 106, 80
Eggenberger A., Udry S., Mazeh T., Segal Y., Mayor M., 2007, A&A, 466, 1179
ESA, 1997, The Hipparcos and Tycho Catalogues, ESA SP-1200
Flower P. J., 1996, ApJ, 469, 355
Frink S., Mitchell D. S., Quirrenbach A., Fischer D. A., Marcy G. W., Butler R. P., 2002, ApJ, 576, 478
Fuhrmann K., 2004, AN, 325, 3
Fuhrmann K., Chini R., 2012, ApJS, 203, 30
Goździewski K., Slonina M., Migaszewski C., Rozenkiewicz A., 2013, MNRAS, 430, 533
Gray D. F., 1982, ApJ, 255, 200
Gray D. F., 1983, PASP, 95, 252
Gray D. F., 1992, The Observation and Analysis of Stellar Photospheres, 2nd ed., Cambridge University Press
Gray D. F., 1994, PASP, 106, 1248
Gray D. F., 1997, Nature, 385, 795
Gray D. F., Baliunas S. L., 1995, ApJ, 441, 436
Gray D. F., Brown K., 2001, PASP, 113, 723
Gray D. F., Brown K. I. T., 2006, PASP, 118, 1112
Gray D. F., Hatzes A. P., 1997, ApJ, 490, 412
Gray D. F., Johanson H. L., 1991, PASP, 103, 439
Gray D. F., Livingston W. C., 1997, ApJ, 474, 798
Gray R. O., Corbally C. J., Garrison R. F., McFadden M. T., Bubar E. J., McGahee C. E., O'Donoghue A. A., Knox E. R., 2006, AJ, 132, 161
Hatzes A. P., 2002, AN, 323, 392
Hatzes A. P., 2013, ApJ, 770, 133
Hatzes A. P., Cochran W. D., 2000, AJ, 120, 979
Hatzes A. P., Cochran W. D., Bakker E. J., 1998, ApJ, 508, 380
Hatzes A. P. Cochran W. D.,Endl M., McArthur B, Paulson D. B.,Walker G. A. H., Campbell B., Yang S., 2003, ApJ, 599, 1383
Hearnshaw J. B., Barnes S. I., Kershaw G. M., Frost N., Graham G., Ritchie R., Nankivell G. R., 2002, Experimental Astronomy, 13, 59
Hekker S., Reffert S., Quirrenbach A., Mitchell D. S., Fischer D. A., Marcy G. W., Butler R. P., 2006, A&A, 454, 943
Henry G. W., Fekel F. C., Henry S. M., Hall D. S., 2000, ApJS, 130, 201
Houk N., Cowley A. P., 1975, Michigan Catalogue of Two Dimentional Spectral Types for the HD Stars. (Vol.1, $-90^\circ < \delta < -53^\circ$)', Univ. of Michigan, Ann Arbor
Hünsch M., Schmitt J. H. M. M., Schröder K.-P, Reimers D., 1996, A&A, 310, 801
Järvinen S. P., Berdyugina S. V., Strassmeier K. G., 2005, A&A, 440, 735
Jofré E., Petrucci R., Saffe C., Saker L., de la Villarmois E. A., Chavero C., Gómez M., Mauas P. J. D., 2015, A&A, 574, 50

Kley W., 2010, in Goździewski K., Niedzielski A., Schneider J., eds, EAS Publications Series Vol. 42, The formation of massive planets in binary star systems. p. 227
Kovtyukh V. V., 2007, MNRAS, 378, 617
Kovtyukh V. V., Gorlova N. I., 2000, A&A, 358, 587
Kovtyukh V. V., Soubiran C., Belik S. I., Gorlova N. I., 2003, A&A, 411, 559
Kovtyukh V. V., Soubiran C., Bienaymé O., Mishenina T. V., Belik S. I., 2006, MNRAS, 371, 879
Kratter K. M., Perets H. B., 2012, ApJ, 753, 91
Kurtz D. W., 2006, in Sterken C., Aerts C., eds, ASP Conference Series, Vol. 349, 101
Kurucz R. L., 2007, Robert L. Kurucz on-line database of observed and predicted atomic transitions
Kurucz R. L., 2009, Robert L. Kurucz on-line database of observed and predicted atomic transitions
Kurucz R. L., 2013, Robert L. Kurucz on-line database of observed and predicted atomic transitions
Lee J. W., Kim S-L., Kim C-H., Koch R. H., Lee C-U., Kim H-I., Park J-H., 2009, AJ, 137, 3181
Mayor M., Queloz D. A., Nature, 378, 355
McWilliam A., 1990, ApJS, 74, 1075
Mermilliod J.-C, 1991, 'Catalogue of Homogeneous Means in the UBV System', Vizier: II/168/ubvmeans
Morais M. H. M., Correia A. C. M., 2012, MNRAS, 419, 3447
Mugrauer M., Neuhäuser R., Mazeh T., Alves J., Guenther E., 2004, A&A, 425, 249
Nardetto N., Mourard D., Kervella P., Mathias Ph., Mérand A., Bersier D., 2006, A&A, 453, 309
Narita N., Sato B., Hirano T., Tamura M., PASJ, 2009, 61, L35
O'Neal, D., 2006, ApJ, 645, 659
Paardekooper S.-J., Thébault P., Mellema G., 2008, MNRAS, 386, 973
Padgett, D. L., 1996, AJ, 471, 847
Patience J. et al., 2002, ApJ, 581, 654
Pourbaix D. et al., 2004, A&A, 424, 727
Press W. H., Teukolsky S. A., Vetterling W. T., Flannery B. P., 2002, Numerical Recipes in C: The Art of Scientific Computing, Cambridge Uni. Press, New York
Pugh T., Gray D. F., 2013, AJ, 145, 38
Quarles B., Cuntz M., Musielak Z. E., 2012, MNRAS, 421, 2930
Queloz D. et al., 2000, A&A, 354, 99
Queloz D., et al., 2001, A&A, 379, 279
Rafikov R. R., Silsbee K., 2015, ApJ, 798, 70
Raghavan D., Henry T. J., Mason B. D., Subasavage J. P., Jao W-C., Beaulieu T. D., Hambly N. C., 2006, ApJ, 646, 523
Ramírez I., Meléndez J., 2005, ApJ, 626, 465
Ramm D. J., 2004, PhD thesis, Univ. Canterbury
Ramm D. J., Pourbaix D., Hearnshaw J. B., Komonjinda S., 2009, MNRAS, 394, 1695
Reffert S., Bergmann C., Quirrenbach A., Trifonov T., Künstler A., 2015, A&A, 574, 116
Roell T., Neuhäuser R., Seifahrt A., Mugrauer M., 2012, A&A, 542, 92
Rowe J. F. et al., 2014, ApJ, 784, 45
Setiawan J. et al., 2003, A&A, 398, L19
Skuljan J., 2004, in Kurtz D. W., Pollard K., eds, Proc. IAU Coll. 193, Variable Stars in the Local Group, p. 575
Slee O. B., Stewart R. T., Bunton J. D., Beasley A. J., Carter B. D., Nelson G. J., 1989, MNRAS, 239, 913
Strassmeier K.G., Schordan P., 2000, AN, 321, 277
Thalmann C. et al., 2014, A&A, 572, 91
Thébault P., 2011, CeMDA, 111, 29
Tokovinin A., Thomas S., Sterzik M., Udry S., 2006, A&A, 450, 681
Tokovinin A., Hartung M., Hayward T. L., 2010, AJ, 140, 510
Toner C. G., Gray D. F., 1988, ApJ, 334, 1008
Trilling D. E., et al., 2007, ApJ, 658, 1264
Tsantaki M., Sousa S. G., Adibekyan V. Zh., Santos N. C., Mortier A., Israelian G., 2013, A&A, 555, 150
Udry S., Mayor M., Queloz D., 1999, in Hearnshaw J. B., Scarfe C. D. eds, Proc. IAU Coll. 170, Precise stellar radial velocities, p. 367
van Leeuwen F., 2007, A&A, 474, 653
Walker G. A. H., Yang. S., Campbell B., Irwin A. W., 1989, ApJ, 343, L21
Walker G. A. H., Bohlender D. A., Walker A. R., Irwin A. W., Yang S. L. S., Larson A., 1992, ApJ, 396, L91
Warner B., 1969, MNRAS, 144, 333
Winn J. N., Johnson J. A., Albrecht S., Howard A. W., Marcy G.,W., Crossfield I. J., Holman M. J., 2009, ApJ, 703, L99
Zucker S., Mazeh T., Santos N. C., Udry S., Mayor M., 2004, A&A, 426, 695